Arch. Metall. Mater. **63** (2018), 4, 1915-1922

DOI: 10.24425/amm.2018.125124

W. WOŁCZYŃSKI*#

NATURE OF SEGREGATION IN THE STEEL STATIC AND BRASS CONTINUOUSLY CAST INGOTS

Experimental observations of the steel morphology as well as measurements of the solutes concentration in the macro-scale were made on the basis of the vertical cut at the mid-depth of the 15-tons steel forging ingot serially produced in one of the steel plant in Poland. Experimental observations of the morphology accompanied by the measurements of the *Peclet Number* were also made on the cross-section of the continuously cast brass ingots serially produced in the copper / brass industry in Poland. The performed measurements allowed to work out some maps of the alloying elements segregation for the longitudinal section of the steel static ingot and a Growth Law for the columnar grains formation in the brass ingots. The marginal stability criterion has been applied to the last mentioned development / description. Some suggestions for the micro-segregation measurement mode in the columnar structure are derived.

Keywords: macro-segregation maps, brass ingots morphology, marginal stability criterion, Growth Law for columnar structure formation

1. Introduction

Phenomenon of segregation plays a crucial role in ensuring good properties of a given alloy. The formation of the "A" –, and "V" – segregates receive a significant attention [1,2,10]. The presence of some nonmetallic inclusions in the solidifying steel has also an influence on segregation [3]. However, in some situations, the convection seems to be conductive in diminishing segregation phenomena in the macro-scale [4,5,7]. The formation of macro-segregation phenomena is significantly changed by the CET (columnar into equiaxed structure transformation) [8,12,15,16]. The shrinkage cavity seems to be the most undesirable product of the segregation [2,9,14].

The phenomenon of macro-segregation has also a connection with the micro-segregation [11,13,17]. Unfortunately, the mentioned analyses consider both extreme cases of solidification: non-equilibrium solidification (the so-called *Scheil* – model) and equilibrium solidification (the so-called Lever Rule), only. It is evident that the use of an universal model for micro-segregation [18,19], and its development for multi-component steel [6], would be more effective / exact in the prediction of micro-segregation / redistribution profiles. The significance of the micro-segregation (and resulting solute redistribution) and its effect upon macro-segregation is well known [20-22].

Eventually, different flows which appear during an ingot solidification result in the nature of macro-segregation [13-16]. However, it should be mentioned that the virtual "switching point" can also be taken into account for the static ingot morphology [23]. At the beginning of the equiaxed structure appearance the viscosity gradient succors to form both sedimentary cones at the static ingot centerline but inside the solid shell (columnar structure shell). At a characteristic ingot height / diameter ratio, the thermo-phoretic "positive" force becomes stronger than the viscosity gradient. Starting from this virtual point, the growing equiaxed grains behave as if they were the "thermal dipoles" and therefore they have tendency to move towards the colder zone (solid shell). In this period of solidification the U-shape shells composed of the equiaxed grains are formed sequentially.

However, the created equiaxed grains are always subjected to gravity. Therefore the so-called "crystal rain" is to be observed especially during activity of the viscosity gradient [23].

Both the viscosity gradient and thermo-phoretic force, accompanied by gravity, ultimately result in the final macro-segregation maps of the chemical elements of steel in the static ingot. The experimentally measured macro-segregation maps are shown in the current study for the vertical section of the steel static ingot. These maps could be a good contribution /matrix towards their reproductions through a numerical simulation of the transport phenomena.

In the case of the continuously cast brass ingots the phenomenon of segregation is important in the micro-scale. Particularly, columnar structure plays a dominant role in the brass ingot solidification [24]. It is concluded that the columnar grains and additionally a single crystal situated axially are conducive to push the insoluble inclusions / hard particles towards the end of a given brass ingot. Thus, some predictions of the ingot morphol-

* INSTITUTE OF METALLURGY AND MATERIALS SCIENCE, POLISH ACADEMY OF SCIENCES, 25 REYMONTA STR., 30 059 KRAKÓW, POLAND

Corresponding author: w.wolczynski@imim.pl

ogy ratio of the columnar to equiaxed structure contribution are an important factor for the insoluble inclusions / hard particles elimination from the continuously cast brass ingots.

Formation of the columnar structure in the continuously cast brass ingot is governed by a proper Growth Law all the more so as the ingot solidification occurs in the stationary state except of the initial transient period of its casting [25]. The current formulation of the Growth Law for the columnar structure formation has been preceded by both the *Peclet Number* measurement within the brass ingot structure and the application of the marginal stability criterion.

2. Morphology and macro-segregation maps of the steel static ingot

Experimental observations of the steel morphology and some elements macro-segregation were made due to the vertical cut at the mid-depth of the 15-ton forging steel ingot serially cast by one of the steel plant in Poland. The examined steel ingot contained 0.32 C, 0.79 Mn, 0.28 Si, 0.009 P, 0.007 S, 0.9 Cr, 0.8 Ni, and 0.36 Mo [wt.%]. Some examples of the examined steel morphologies are shown in Fig. 1, and macro-segregation maps in Fig. 2.

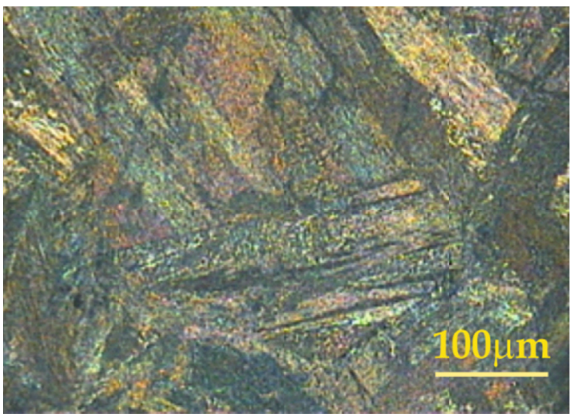

Fig. 1a. Columnar grains within the area of the constrained solidification

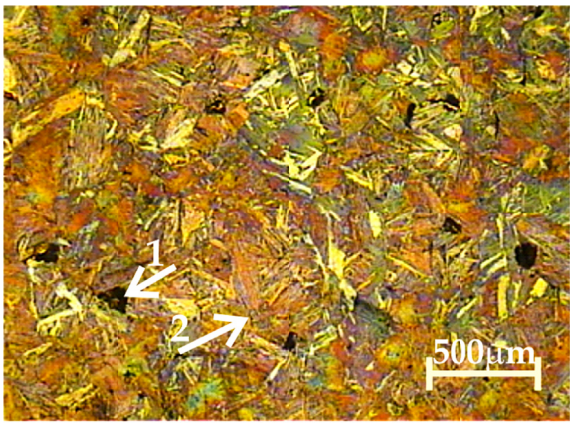

Fig. 1b. Equiaxed grains (arrow 1 shows the large carbide – macro-segregation; arrow 2 shows the carbide precipitate surrounding a given grain – micro-segregation)

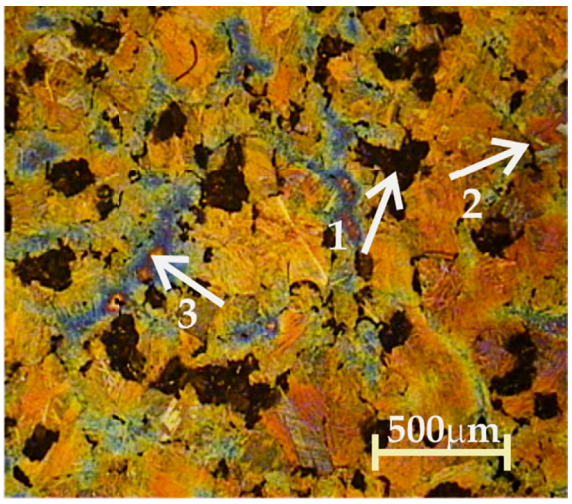

Fig. 1c. Intensive macro-segregation at the ingot centerline (arrow 1 shows the large carbide – macro-segregation; arrow 2 shows the carbide precipitate surrounding a given grain – micro-segregation; arrow 3 (blue area) shows the micro-shrinkage and porosity – macro-segregation)

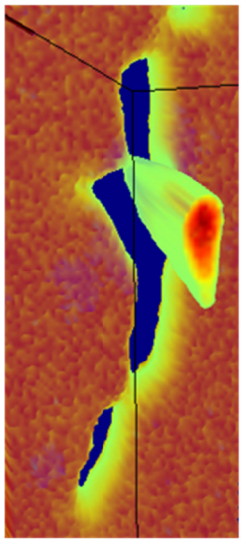

Fig. 1d. Stalagmite / grain growing inside the extremely developed void revealed at the ingot centerline (scanning acoustic microscopy)

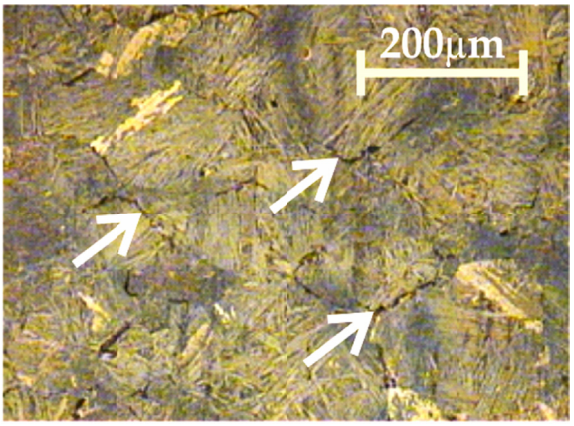

Fig. 1e. Columnar and equiaxed grains co-existing within the $C \rightarrow E$ zone; (arrows show the carbide precipitate surrounding a given grain – micro-segregation)

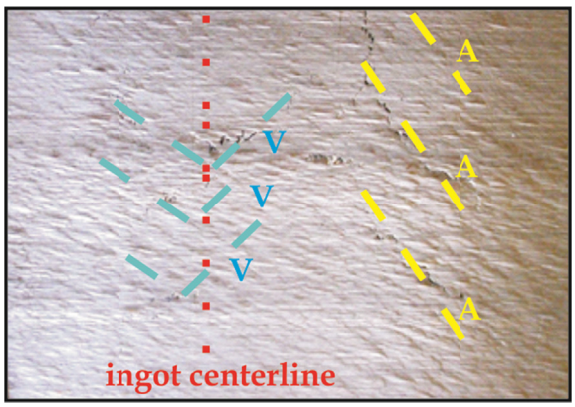

Fig. 1f. "A",– and "V" – segregates (dashed lines are superposed over the detected micro-fissures)

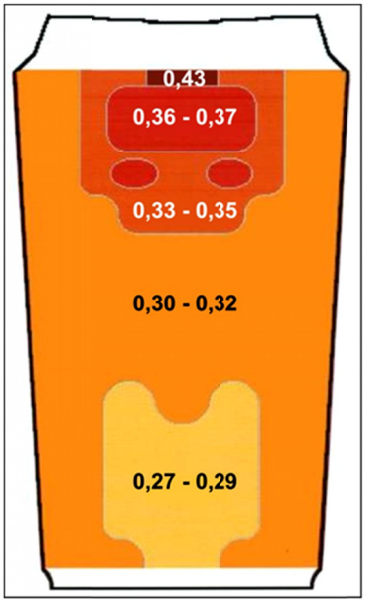

Fig. 2a. Macro-segregation pattern of carbon

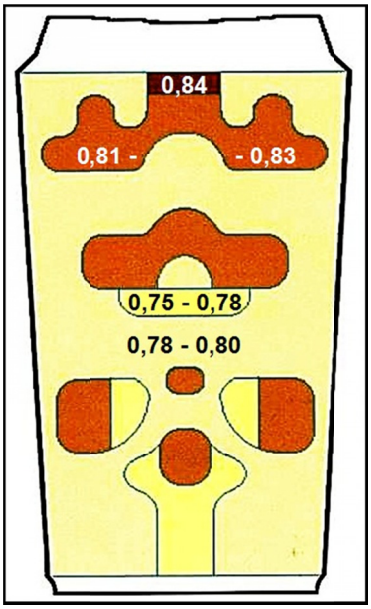

Fig. 2b. Macro-segregation pattern of manganese

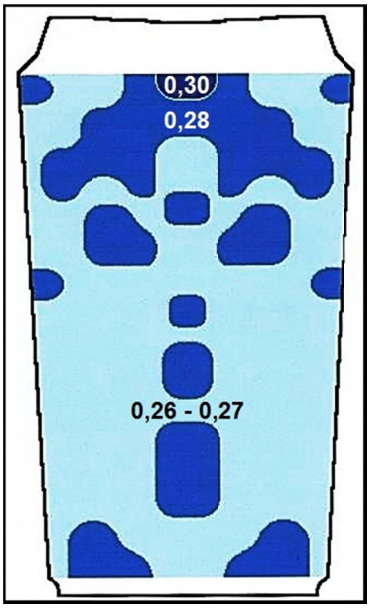

Fig. 2c. Macro-segregation pattern of silicon

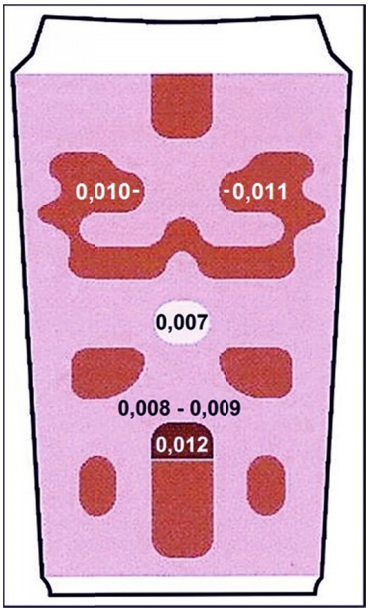

Fig. 2d. Macro-segregation pattern of phosphorus

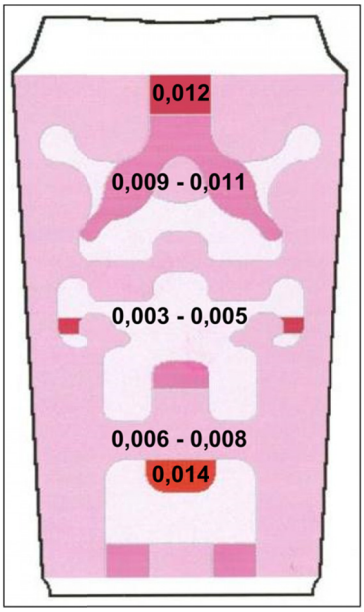

Fig. 2e. Macro-segregation pattern of sulfur

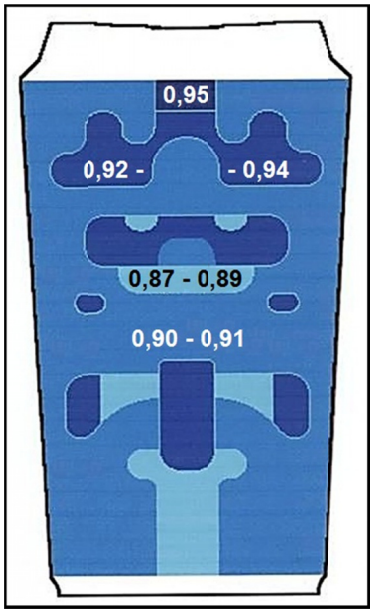

Fig. 2f. Macro-segregation pattern of chromium

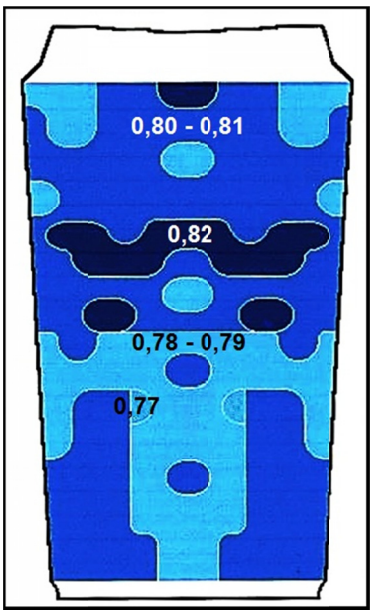

Fig. 2g. Macro-segregation pattern of nickel

3. Brass ingot morphology and resulting Growth Law

The delivered observations of the steel static ingot morphology confirm the intensive appearance of both macro-segregation and also micro-segregation. Particularly, macro-segregation plays an essential role in the materials properties of an ingot and a subsequent plastic deformation.

On the other hand, some observations of the brass ingot morphology confirm that, first of all, the columnar structure is formed during continuous casting, Fig. 3. Thus, it is justified to measure the *Peclet Number* within the brass ingot morphology and work out a resulting Growth Law.

Fig. 3a. Two types of columnar (FC – fine columnar and C – columnar) structure revealed on the brass ingot cross-section

The mentioned *Peclet* Number results directly from the measurement / estimation of the R_{exp} – tip radius of the columnar dendrite or columnar cells revealed on the longitudinal and

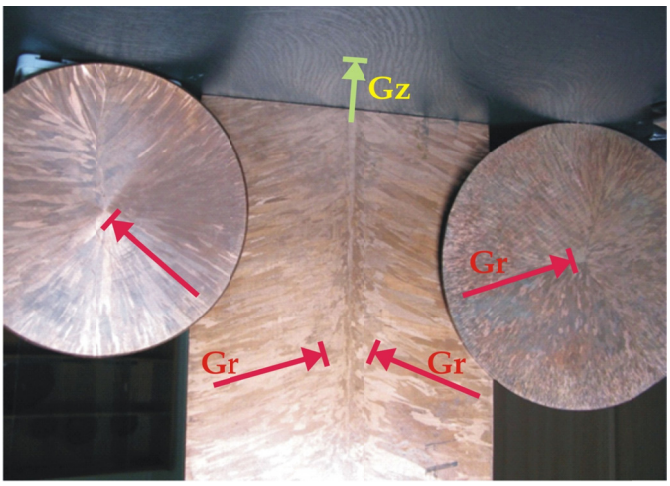

Fig. 3b. Interplay between columnar structure formation / situation and thermal gradient localization; G_r – radial thermal gradient operating during columnar structure formation, G_Z – vertical / axial thermal gradient operating during single crystal growth

Fig. 3c. Approximate method of the R_{exp} – tip radius measurement within the columnar structure surrounding the single crystal situated axially in the brass ingot

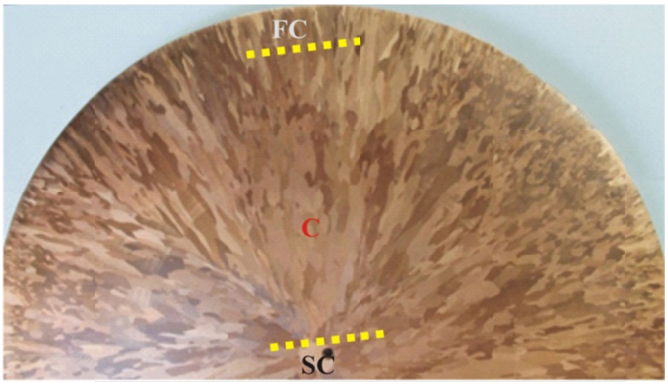

Fig. 3d. Columnar structure and single crystal as the dominant morphology within the brass ingot; FC – fine columnar, C – columnar, and SC – single crystal as revealed

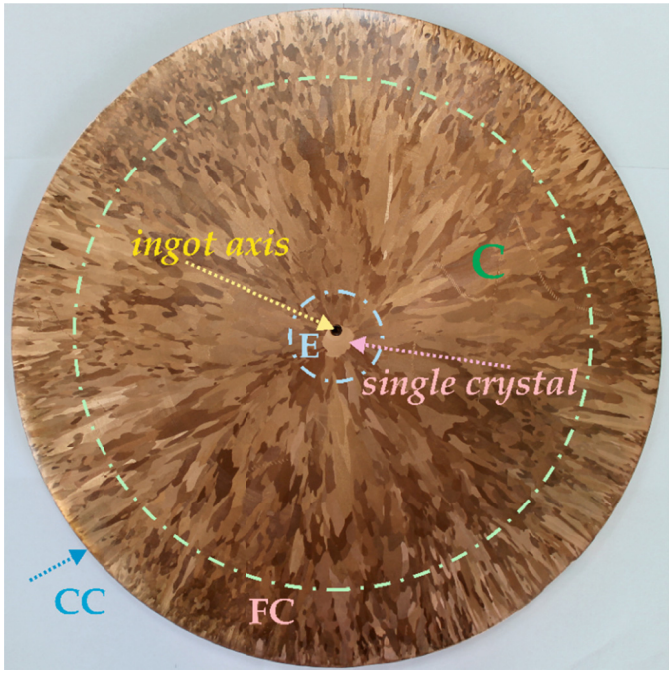

Fig. 3e. Co-existence of: CC – chilled columnar, FC – fine columnar, C – columnar, E – equiaxed structure and SC – single crystal situated axially

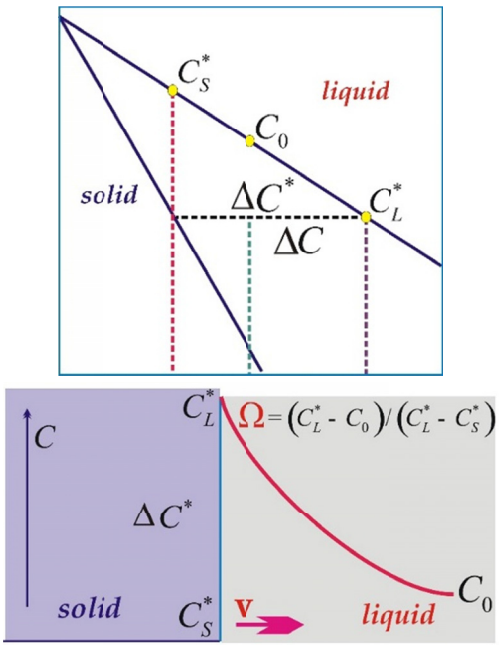

Fig. 4. Definition of the Ω – supersaturation applied to Eq. (2); C_0 is the nominal Zn-solute concentration in a given brass; C_L^*, C_S^* are the Zn-solute concentrations in the liquid and the solid, respectively, as observed at the s/l interface moving with the v_C – velocity (stationary solidification), [28]; a) arbitrary phase diagram, b) solute profile at the s/l interface

transversal sections of an ingot, Fig. 3c. The definition of the *Pe – Peclet* Number (for the Zn-solute diffusion in brass columnar structure) is as follows, [26]:

$$Pe = \frac{v_C \, R_{\exp}}{2\,D} \tag{1}$$

v_C is the velocity of the moving s/l interface of columnar structure; D – diffusion coefficient.

The *Pe – Peclet* Number is usually greater than unity but sometimes can be less. In the last-mentioned case it is sufficient to use the so-called I_2 – second term of the *Ivantsov's* function development, [27]. This term is equal to the Ω – supersaturation governing the tip radius formation, Fig. 4:

$$I_2 = 2Pe/(2Pe+1) = \Omega \tag{2a}$$

The dendrite / cell tip radius grows at the limit of stability, [29], that is, at the marginal stability, [30]:

$$\lambda_i = R_{th} = 2\pi\,\sigma_E^{\,0.5}\left[\Delta S\,(m\,G_C - G)\right]^{-0.5} \tag{3}$$

λ_i is the perturbation wavelength for the marginal stability, σ_E – specific surface free energy, ΔS entropy of fusion, m – slope of the liquidus line, G_C – solute concentration gradient at the columnar dendrite / cell tip, G – thermal gradient at a columnar dendrite / cell tip.

It is justified to admit that theoretically predicted tip radius and experimentally estimated tip radius are equal to each other, $R_{th} \equiv R_{\exp} \equiv \bar{R}$. Eq. (3) yields:

$$\Omega = \frac{C_L^* - C_0}{C_L^* - C_S^*} \rightarrow C_L^* = C_0/\left(1+\Omega(k-1)\right) \tag{4}$$

with $C_S^* = kC_L^*$, at the s/l interface, Fig. 4. Thus, it results from Eq. (2a) that:

$$I_2 = 2Pe/(2Pe+1) = \left(C_L^* - C_0\right)\left[(1-k)C_L^*\right]^{-1} \tag{5}$$

Eq. (3) can be rewritten as follows:

$$\lambda_i = 2\pi\sqrt{\sigma_E\,\Delta S^{-1}/\left\{\frac{v_C}{D}\left[(k-1)\frac{C_0}{1-(1-k)I_2}\right]m - G\right\}} \tag{6}$$

where $G_C = dC/dz = -v_C\,(1-k)\,C_L^*/D$.

When, according to (Eq. (3)):

$$A = (R_{th})^2\left[m\,G_C - G\right] = 4\pi^2\sigma_E\,(\Delta S)^{-1} \tag{7}$$

then, l.h.s of Eq. (7) can be rewritten as:

$$A = (R_{th})^2\left[m\frac{v_C}{D}(k-1)\,C_L^* - G\right] \tag{7a}$$

$$A = (R_{th})^2\left[m\frac{v_C}{D}(k-1)\frac{C_0}{1-(1-k)I_2} - G\right] \tag{7b}$$

with $I_2 = 2\,Pe/(2\,Pe+1) = \dfrac{v_C R_{th}}{R_{th}\,v_C + D}$.

Subsequently,

$$A = (R_{th})^2\left[m\frac{v_C}{D}(k-1)\frac{C_0}{1-(1-k)v_C\dfrac{R_{th}}{R_{th}v_C+D}} - G\right] \tag{7c}$$

$$A=\left(\hat{R}\right)^2\left[m\frac{v_C\left(k-1\right)C_0}{D\left[\frac{\hat{R}v_C+D-\left(1-k\right)\hat{R}v_C}{\hat{R}v_C+D}\right]}-G\right],$$

with $R_{th}\equiv R_{\exp}\equiv\hat{R}$ (7d)

$$A=\hat{R}^2\left[m\frac{v_C\left(k-1\right)C_0\left(\hat{R}v_C+D\right)}{D\left(D+k\hat{R}v_C\right)}-G\right] \quad (7e)$$

Eq. (7) may be transformed into:

$$\hat{R}^2\left[m\,v_C\left(k-1\right)C_0\left(\hat{R}v_C+D\right)-G\,D\left(D+k\,\hat{R}v_C\right)\right]$$
$$=\frac{4\,\pi^2\sigma_E}{\Delta S}D\left(D+k\,\hat{R}v_C\right) \quad (8)$$

After some rearrangements Eq. (8) becomes:

$$\hat{R}^3\left[\Delta S\,v_C\left(m\left(k-1\right)C_0\,v_C-G\,D\,k\right)\right]$$
$$+\hat{R}^2\left[\Delta S\,D\left(m\,v_C\left(k-1\right)C_0-G\,D\right)\right]$$
$$-\hat{R}\left[4\,\pi^2\,\sigma_E\,D\,k\,v_C\right]-4\,\pi^2\,\sigma_E\,D^2=0 \quad (9a)$$

where k is partition ratio.

Eq. (9a) presents the Growth Law for the very small Pe – *Peclet* Number (less than unity).

However, when the Pe – *Peclet* Number is properly greater, then, the higher development of the *Ivantsov's* function is to be applied:

$$I_3=Pe\left(Pe+3\right)/\left(Pe^2+4Pe+2\right)=\Omega \quad (2b)$$

$$I_4=Pe\left(3\,Pe+5\right)/\left(3\,Pe^2+8Pe+2\right)=\Omega \quad (2c)$$

then, the adequate versions of the Growth Law develop suitably:

$$\hat{R}^4\left[\Delta S\,{v_C}^2\left(m\left(k-1\right)C_0\,v_C-G\,D\,k\right)\right]+$$
$$\hat{R}^3\left[\Delta S\,D\,v_C\left(8\,m\,v_C\left(k-1\right)C_0-G\,D\left(2+6k\right)\right)\right]+$$
$$\hat{R}^2\left[\Delta S\,D^2\left(8\,m\,v_C\left(k-1\right)C_0-8\,G\,D\right)-4\,\pi^2\sigma_E\,D\,k\,{v_C}^2\right]-$$
$$\hat{R}\left[4\,\pi^2\,\sigma_E\,v_C\,D^2\left(2+6k\right)\right]-32\,\pi^2\,\sigma_E\,D^3=0 \quad (9b)$$

$$\hat{R}^4\left[3\,\Delta S\,{v_C}^2\left(G\,D\,k-m\,v_C\left(k-1\right)C_0\right)\right]+$$
$$\hat{R}^3\left[2\,\Delta S\,D\,v_C\left(G\,D\left(5\,k+3\right)-8\,m\,v_C\left(k-1\right)C_0\right)\right]+$$
$$\hat{R}^2\left[8\,\Delta S\,D^2\left(G\,D-m\,v_C\left(k-1\right)C_0\right)+12\,\pi^2\sigma_E\,D\,k\,{v_C}^2\right]+$$
$$\hat{R}\left[8\,\pi^2\,\sigma_E\,v_C\,D^2\left(3+5k\right)\right]+32\,\pi^2\,\sigma_E\,D^3=0 \quad (9c)$$

Eq. (9) means that at a given vertical rate of the ingot displacement along the crystallizer, with the accompanying growth rate of columnar structure, v_C, and at a given thermal gradient imposed at the s/l interface, G, with the nominal Zn – solute concentration in the brass, C_0, the one and only one resultant tip radius, $\hat{R}$ (also size of the grain) can be expected in the ingot morphology.

4. Methods of the micro-segregation measurement

In the case of the steel static ingots the macro-segregation is the important factor for the estimation of materials properties. It is obvious that in the case of the continuously cast brass ingots not only size of the structure (especially size of the columnar structure) plays an essential role in the estimation of final properties of a given product but the micro-segregation as well. Thus, the following methods, Fig. 5, are suggested to measure the Zn – solute micro-segregation (the Zn – solute redistribution after back-diffusion, in reality [18]).

The general equation describing the solute redistribution (expressed in mole fraction) after back-diffusion is:

$$N^B\left(x;x_0,\alpha\right)=\left[k+\beta^{ex}\left(x;x_0\right)\beta^{in}\left(x_0,\alpha\right)\right]N^L\left(x;\alpha\right) \quad (10)$$

where, x is the current amount of the growing columnar grain (2D solidification), x_0 – amount of the columnar grain at the moment of freezing, α – back-diffusion parameter, β^{ex} – coefficient of the extent of the solute redistribution, β^{in} – coefficient of the intensity of the solute redistribution, $\bar{L}$ – half the diameter of the columnar grain, $\bar{H}$ – height of the frozen columnar grain being in the contact with the surrounded liquid just before the appearance of precipitates, N^L – current solute concentration in the solidifying alloy, [18].

a) at the bottom of a frozen columnar grain (cell / dendrite) or on the columnar grain cross-section (without freezing),

$$N^B\left(x;1,\alpha\right)=\left[k+\beta^{ex}\left(x;1\right)\beta^{in}\left(1,\alpha\right)\right]N^L\left(x;\alpha\right) \quad (10a)$$

b) at a certain height of a frozen columnar grain,

$$N^B\left(x;x_0\left(\bar{L}_0\right),\alpha\right)$$
$$=\left[k+\beta^{ex}\left(x;x_0\left(\bar{L}_0\right)\right)\beta^{in}\left(x_0\left(\bar{L}_0\right),\alpha\right)\right]N^L\left(x;\alpha\right) \quad (10b)$$

c) along the axis of symmetry of a frozen columnar grain,

$$N^B\left(0;x_0,\alpha\right)$$
$$=\left[k+\beta^{ex}\left(0;x_0\right)\beta^{in}\left(x_0,\alpha\right)\right]N^L\left(0,\alpha\right) \quad (10c)$$

d) along the envelope of a frozen columnar grain,

$$N^B\left(x_0;x_0,\alpha\right)$$
$$=\left[k+\beta^{ex}\left(x_0;x_0\right)\beta^{in}\left(x_0,\alpha\right)\right]N^L\left(x_0,\alpha\right) \quad (10d)$$

5. Concluding remarks

The segregation phenomena are important for both static steel ingot and continuously cast brass ingot from the viewpoint of materials properties, especially when the ingots are subjected to plastic deformation.

However, the macro-segregation plays an essential role in the case of the static steel ingot, Fig.1b, Fig. 1c, Fig. 1f, Fig. 2, whereas the micro-segregation (Zn – solute redistribution, Eq. 10) is expected when the dominant columnar structure is formed within the continuously cast brass ingot, Fig. 3.

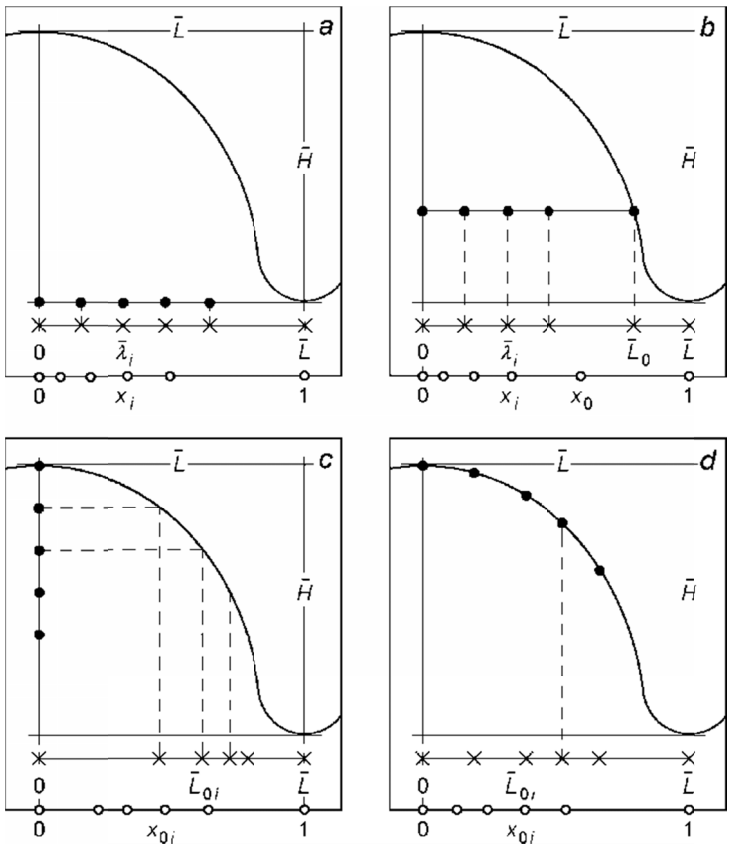

Fig. 5. Fundamental methods of the solute redistribution measurement (points) for the frozen columnar cell or columnar dendrite (with the solidification arrested)

The macro-segregation maps, Fig. 2, may be described by the so-called macro-segregation index defined as:

$$i_{macr.} = \left(N^B_{\max} - N^B_{\min} \right) / N_0 \tag{11}$$

$N^B_{\max}$, $N^B_{\min}$ are the maximum / minimum solute redistribution in a given area of the steel static ingot, respectively, N_0 – nominal solute mole fraction in a given steel.

Since the columnar structure is dominant in the continuously cast brass ingots, thus, the measurements / estimations of the *Peclet Number* were performed within the brass ingots structure, Fig. 3c. These measurements allowed to formulate some versions of the Growth Law, Eq. (9), with the use of the marginal stability criterion, Eq. (3), and definition of the *Ivanstov's* function, Eq. (2).

The formulated Growth Law, Eq. (9), has a physical meaning:

the growth of the columnar structure in the brass ingot solidifying under stationary state occurs in the way ensuring the tip radius to be marginally stable against some perturbations of solute redistribution field or thermal gradients field.

Acknowledgements

The support was provided by the National Centre for Research and Development under Grant No. PBS3/A5/52/2015.

REFERENCES

[1] K. Suzuki, K. Taniguchi, Transaction of the Iron and Steel Institute of Japan **21** (4) 235-242 (1981).

[2] J. Moore, N. Shah, International Metals Review **28**, 338-356 (1983).

[3] T. Matsumiya, Materials Transactions of the Japan Institute of Metals **33** (9) 783-794 (1992).

[4] J.P. Gu, C. Beckermann, Metallurgical and Materials Transactions **30A**, 1357-1366 (1999).

[5] Y.M. Won, B.G. Thomas, Metallurgical and Materials Transactions **32A**, 1755-1767 (2001).

[6] T. Himemiya, W. Wołczyński, Materials Transactions of the Japan Institute of Metals **43** (11), 2890-2896 (2002).

[7] G. Guillemont, Ch.A. Gandin, H. Combeau, The Iron and Steel Institute of Japan – International **46**, 880-895 (2006).

[8] M. Wu, A. Ludwig, Metallurgical and Materials Transactions **38A**, 1465-1475, (2007).

[9] L. Nastac, Metallurgical Transactions **42B**, 1231-1243 (2011).

[10] J. Li, M. Wu, J. Hao, A. Ludwig, IOP Conf. Series: Materials Science and Engineering **27**, 012055 (2012).

[11] M. Wu, J. Li, A. Ludwig, A. Kharicha, Computational Materials Science **79**, 830-840 (2013).

[12] W.U. Mirihanage, H. Dai, H. Dong, D.J. Browne, Advanced Engineering Materials **15** (4) 216-229 (2013).

[13] M. Wu, J. Li A. Ludwig, A. Kharicha, Computational Materials Science **92**, 267-285 (2014).

[14] M. Wu, A. Kharicha, A. Ludwig, IOP Conf. Series: Materials Science and Engineering **84**, 012006 (2015).
[15] M. Wu, Y. Zheng, A. Kharicha, A. Ludwig, Computational Materials Science **124**, 444-455 (2016).
[16] Y. Zheng, M. Wu, A. Kharicha, A. Ludwig, Computational Materials Science **124**, 456-470 (2016).
[17] Y.M. Won, B.G. Thomas, Metallurgical and Materials Transactions **32A**, 1755-1767 (2001).
[18] W. Wołczyński, Archives of Metallurgy and Materials **60** (3B), 2403-2407 (2015).
[19] W. Wołczyński, Archives of Metallurgy and Materials **60** (3B), 2409-2414 (2015).
[20] A. Roosz, Z. Gacsi, G. Fuchs, Acta Metallurgica **32**, 1745-1754 (1984).
[21] N.F. Dean, A. Mortensen, M.C. Flemings, Metallurgical Transactions **25A**, 2295-2301 (1994).
[22] A. Turkeli, D.H. Kirkwood, Materials Science Forum **508**, 443-448 (2006).
[23] W. Wołczyński, Entry in: The Encyclopedia of Iron, Steel, and Their Alloys, Ed. CRC Press, Taylor & Francis Group, Boca Raton, London, New York, Eds. Rafael Colas, George E. Totten, volume III: Heat Treatment: Special – Molten, 1910-1924 (2016).
[24] W. Wołczyński, A.A. Ivanova, P. Kwapisiński, E. Olejnik, Archives of Metallurgy and Materials **62** (4) 2461-2467 (2017).
[25] W. Wołczyński, Z. Lipnicki, A. W. Bydałek, A.A. Ivanova, Archives of Foundry Engineering **16** (3) 141-146 (2016).
[26] R. Trivedi, Journal of Crystal Growth **49**, 219-232 (1980).
[27] G.P. Ivantsov, Doklady Akademii Nauk SSSR **58**, 567-72 (1947).
[28] W. Kurz, D.J. Fisher, Fundamentals of Solidification, Trans. Tech. Publ. (1984).
[29] B. Caroli, C. Caroli, B. Roulet, Journal of Crystal Growth **76**, 31-49 (1986).
[30] J.S. Langer, H. Muller-Krumbhaar, Journal of Crystal Growth **42**, 11-14 (1977).